

# Standard slot waveguide and double hybrid plasmonic waveguide configurations for enhanced evanescent field absorption methane gas sensing

Muhammad Ali Butt,\* Ryszard Piramidowicz

<sup>1</sup>Warsaw University of Technology, Institute of Microelectronics and Optoelectronics, Koszykowa 75, 00-662 Warszawa, Poland

Received October 12, 2022; accepted March 29, 2022; published March 31, 2022

**Abstract**—Herein, a numerical study is presented on standard slot waveguide and double hybrid plasmonic waveguide based on a silicon-on-insulator platform. The geometric parameters of both waveguides are optimized for an operational wavelength of 3.39  $\mu\text{m}$  (absorption line of methane gas) to obtain the maximum evanescent field ratio (EFR). By utilizing Lambert-Beer's law, the gas sensing capability of both waveguides is determined. It is found out that both waveguides of length 100  $\mu\text{m}$  offer high EFR resulting in the 3dB decay of the propagating mode power for a methane gas concentration of 20-22 % in the chamber. The study provides the foundation for practical realization of compact and highly sensitive gas sensors.

Methane ( $\text{CH}_4$ ) is a colorless, odorless, and flammable gas which has a tendency to form extremely explosive mixtures with air and/or other chemicals [1]. It is also one of the greenhouse gases which emission contribute significantly to atmospheric pollution and global warming. Therefore, it is among those gaseous pollutants which are of specific interest with respect to the development of fast, highly reliable and low-cost sensing/monitoring methods. One of these, based on optical waveguides optimized for 3.39  $\mu\text{m}$  (absorption line of methane), is discussed below.

In general, there is a variety of waveguide (hereafter abbreviated as WG) configurations based on evanescent field (hereafter referred to as EF) phenomenon that can be used to provide gas sensing functionality using different technological platforms [2-5]. Based on the total internal reflection theory, the dielectric WG may guide the light within a high refractive index core. At large WG cross-sections, these WGs feature provides good mode confinement and minimal propagation loss. It is an obvious fact that for obtaining exceptionally sensitive gas sensors the overlap between the evanescent field and the ambient medium should be possibly high [6]. By reducing the WG dimensions, the EF of the propagating mode can be increased at the expense of high propagation loss [7]. It should be noticed that the diffraction effects also limit the WG's ability to confine the light. Plasmonic WGs generate surface plasmon (SP) waves at the dielectric-metal interface, which are evanescently restricted in the

propagation direction [8]. Because their light confining capacity is unaffected by the diffraction limit, these WG arrangements can restrict light to the subwavelength region. Instead, due to the presence of metal as the WG's core element, these WGs have high propagation losses. The hybrid plasmonic WG (HPWG) arrangement can provide a low EF and high propagation loss solution. In this work, we propose two highly sensitive WG configurations, i.e., standard slot WG (referred to as SSWG) and double hybrid plasmonic WG (referred to as DHPWG) for the sensing of  $\text{CH}_4$  gas as shown in Fig.1.

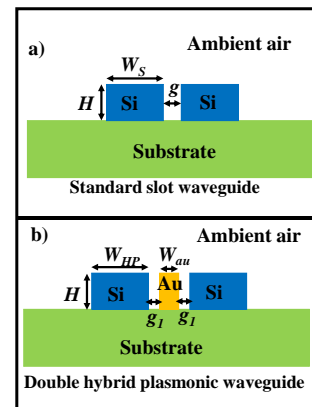


Fig. 1. Graphical illustration of, a) SSWG, b) DHPWG.

The WG geometries are optimized to obtain the optimum evanescent field ratio (EFR) at an operational wavelength of 3.39  $\mu\text{m}$ , which is the absorption line of  $\text{CH}_4$  [9]. The SSWG is composed of two silicon (high index material,  $n=3.47$  @3.39  $\mu\text{m}$ ) strips separated by a subwavelength-scale low-refractive-index (air,  $n=1.0$ ) slot region. The core height of both WGs is represented as  $H$ , which is maintained at 220 nm. For SSWG, the silicon rail width and gap between the rails are expressed as  $W_s$  and  $g$ , respectively. The DHPWG consists of a subwavelength scale metal strip (gold abbreviated as Au is chosen due to its oxidation resistance) placed in the middle of an SSWG. The Au strip is separated on both sides from the silicon rails with a subwavelength low-refractive-index gap (air,  $n=1.0$ ). The width of the silicon strip, Au strip,

\* E-mail: ali.butt@pw.edu.pl

and the gap are denoted as  $W_{HP}$ ,  $W_{Au}$ , and  $g_I$ , respectively. The  $W_{Au}$  is maintained at 80 nm throughout the whole paper. The effective refractive index ( $n_{eff}$ ) and EFR analysis of both structures are carried out via a 2D-finite element method (FEM)-based model in COMSOL Multiphysics 5.5. The device model is divided into triangular mesh elements with an “extremely fine” mesh grid size for the entire geometry. For wave propagation systems, it is anticipated to model a domain with open boundaries of the computational domain as it allows the electromagnetic wave to travel without any reflections. The open geometry is assessed by allocating a scattering boundary condition (SBC) at the outer edges of the simulation window. Every gas has a distinct absorption peak that serves as a kind of standard, unequivocally identifying that gas [10]. When the WG sensor is placed in a gaseous medium, the EF interacting with that gas causes power degeneration of the transmitting mode if it correlates with the measurand gas’s absorption line. The power decay can be articulated using Lambert-Beer’s law, which is usually affected by gas concentration, absorption coefficient, length, and EFR of the WG [11]. As a result, EFR is an imperative factor of the gas sensors realized with the use of the EF absorption mechanism [12]. The EFR is the ratio of the intensity integration of the desired region (upper cladding) to the intensity integration of the total WG structure (core, upper cladding, and lower cladding). The real part of the effective refractive index ( $Re(n_{eff})$ ) of the propagating mode at  $3.39 \mu\text{m}$  in SSWG is calculated for different values of  $g$  and  $W_S$  as shown in Fig. 2a.

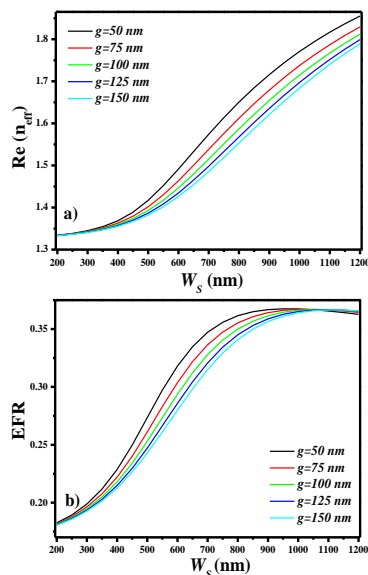


Fig. 2. Characteristics of SSWG, a)  $Re(n_{eff})$  of SSWG versus  $W_S$ , b) EFR of SSWG versus  $W_S$ .

The geometry of the WG should be optimized to have a maximum overlap of the electric field in the low index region. As  $W_S$  increases, the majority of the mode power is confined in the silicon rails, which results in lowering

the mode power in the nano-gap. The EFR of the SSWG geometry is optimized concerning  $W_S$  and  $g$  for an operational wavelength of  $3.39 \mu\text{m}$ , as shown in Fig. 2b. The SSWG geometry offers a maximum EFR  $\sim 0.37$  at  $W_S=950 \text{ nm}$ ,  $g=50 \text{ nm}$ , and  $H=220 \text{ nm}$ . The higher the EFR is, the stronger the light interaction is, with the  $\text{CH}_4$  gas resulting in the fast decay of the propagating mode power due to strong gas absorption.

For the DHPWG configuration, the  $Re(n_{eff})$  of the hybrid mode is calculated with respect to  $W_{HP}$  and  $g_I$  of the WG geometry, as shown in Fig. 3a. The proposed WG scheme supports dual hybrid modes which are confined between the silicon and Au strip. The DHPWG offers a maximum EFR  $\sim 0.415$  at  $W_{HP}=450 \text{ nm}$ ,  $g_I=50 \text{ nm}$ ,  $W_{Au}=80 \text{ nm}$  and  $H=220 \text{ nm}$ , as shown in Fig. 3b. There are two main benefits of the DHPWG geometry compared to that of SSWG. Firstly, EFR is 10% higher than the one offered by SSWG. Secondly, the small dimension of the DHPWG makes it attractive for dense optical WG systems. In the case of SSWG, the maximum EFR ( $\sim 0.37$ ) is obtained for  $W_S=950 \text{ nm}$ , whereas the maximum EFR ( $\sim 0.415$ ) for DHPWG is obtained for  $W_{HP}=450 \text{ nm}$ .

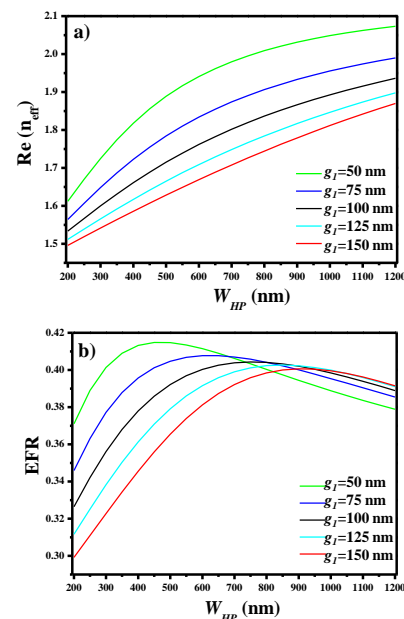


Fig. 3. Characteristics of DHPWG, a)  $Re(n_{eff})$  of DHPWG versus  $W_{HP}$ , b) EFR of DHPWG versus  $W_{HP}$ .

The normalized E-field distribution in the SSWG and DHPWG at optimized geometric parameters are plotted as shown in Fig. 4a and Fig. 4b, respectively. A subwavelength mode with high intensity is confined in the narrow low index region of the SSWG configuration whereas, two hybrid modes are confined in the low index regions in the DHPWG, which provides higher light-matter interaction. From Fig. 4, it can be seen that the width of the optimized SSWG and DHPWG structure is  $1950 \text{ nm}$  and  $1030 \text{ nm}$ , respectively. Moreover, the E-

field line graph of the corresponding WG structures along the dotted white line is also plotted in Fig. 4.

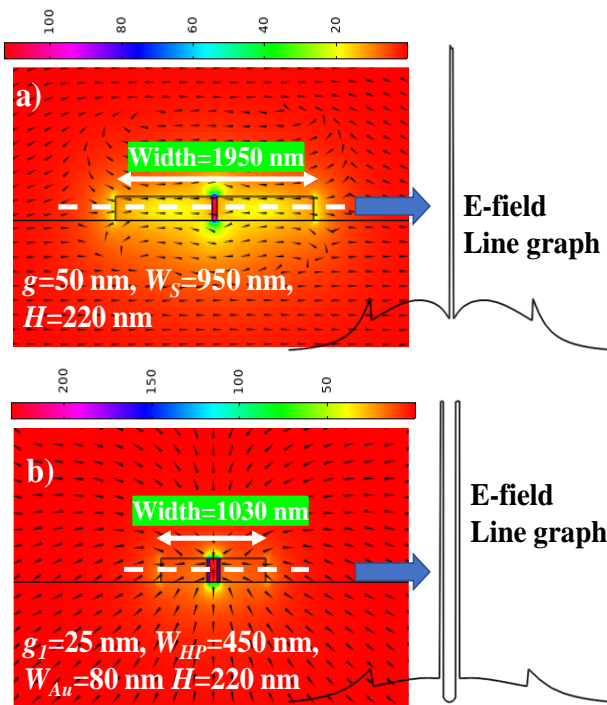


Fig. 4. Normalized E-field distribution in, a) SSWG, b) DHPWG.

To analyze the sensing capabilities of both proposed WG structures, Lambert-Beer's model has been used, which is expressed as:

$$P = P_o e^{-(\eta \cdot \varepsilon \cdot C \cdot L_i)}$$

where  $\eta$  is the EFR of the respective WG,  $\varepsilon$  is the absorption coefficient of CH<sub>4</sub> gas,  $C$  is the gas concentration (0 to 100%), and  $L_i$  is the length of the WG.  $P$  is the output power of the WG, and  $P_o$  is the input power which is fixed at 10 mW. The optimized value of EFR (0.37 for SSWG and 0.415 for DHPWG) is utilized to determine the best sensing performance. The  $\varepsilon$  of CH<sub>4</sub> gas at 3.39  $\mu\text{m}$  of operational wavelength is around 8.3 atm/cm.

The output power decay versus gas concentration is plotted in Fig. 5 for different lengths of the WGs, i.e., 10  $\mu\text{m}$ , 20  $\mu\text{m}$ , 30  $\mu\text{m}$ , 40  $\mu\text{m}$  and 100  $\mu\text{m}$ . The output power of the WGs with  $L=100 \mu\text{m}$  decays faster than  $L=10 \mu\text{m}$ . This is due to the large interaction of the gas with the EF of the WG. The 3dB power decay in SSWG and DHPWG of  $L=100 \mu\text{m}$  is obtained for the CH<sub>4</sub> gas concentration of 20% and 22 %, respectively.

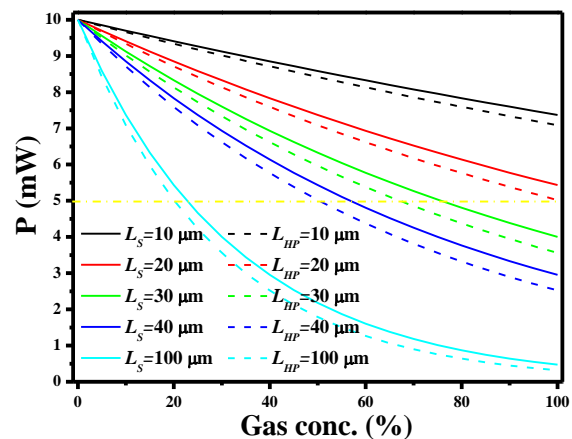


Fig. 5. Output power versus CH<sub>4</sub> gas concentration.

In conclusion, it is stated that both WG configurations proposed in this paper are optimized at 3.39  $\mu\text{m}$  operational wavelength and offer an EFR in the range of 0.37-0.415. When the WG operates at the absorption line of the CH<sub>4</sub> gas, i.e., 3.39  $\mu\text{m}$ , the propagating mode power suffers a reduction which depends on the EFR, gas concentration, length of the WG and the absorption coefficient of the CH<sub>4</sub> gas. It is determined that both WGs of 100  $\mu\text{m}$  length suffer a 3dB decrease of the propagating mode power for the CH<sub>4</sub> gas concentration of 20-22 % in the chamber. This proves their highly sensitive nature and potential for sensing applications.

The research is co-financed by the Foundation for Polish Science from the European Regional Development Fund within the project POIR.04.04.00-00-14D6/18 "Hybrid sensor platforms for integrated photonic systems based on ceramic and polymer materials (HYPHa)" (TEAM-NET program).

## References

- [1] J.Y. Yo, Y.S. Kwon, J.W. Lee, J.S. Park, B.H. Rho, W.II. Choi. Tuberculosis and Respiratory Diseases **74**, 120 (2013).
- [2] M.A. Butt, S.A. Degtyarev, S.N. Khonina, N.L. Kazanskiy, J. Modern Opt. **64**, 1892 (2017).
- [3] M.A. Butt, S.N. Khonina, N.L. Kazanskiy, Optik **168**, 692 (2018).
- [4] M.A. Butt, S.N. Khonina, S.N. Kazanskiy. J. Modern Opt. **65**, 174 (2017).
- [5] S.N. Khonina, N.L. Kazanskiy, M.A. Butt. IEEE Sensors J. **20**, 8469 (2020).
- [6] M.Vlk, A. Datta, S. Alberti, H.D. Yallev, V. Mittal, G.S. Murugan, J. Jagerska, Light: Science Appl. **10**, 26 (2021).
- [7] M.A. Butt, S.N. Khonina, N.L. Kazanskiy. Laser Phys. **29**, 076202 (2019).
- [8] M.A. Butt, N.L. Kazanskiy, S.N. Khonina, Current Appl. Phys. **20**, 1274 (2020).
- [9] T. Milde, M. Hoppe, H. Tatenguem, C. Assmann, W. Schade, J. Sacher. Appl. Opt. **58**, C84 (2019).
- [10] N.L. Kazanskiy, S.N. Khonina, M.A. Butt. Photonic Sensors **11**, 279 (2021).
- [11] D. Popa, F. Udrea. Sensors **19**, 2076 (2019).
- [12] S-W. Kang, K. Sasaki, H. Minamitani, Appl. Opt. **32**, 3544 (1993).